Carbon 216 (2024) 118502

Contents lists available at ScienceDirect

Carbon

journal homepage: www.elsevier.com/locate/carbon

Research article

Transmission through graphene of electrons in the 30 – 900 eV range

Alice Apponi [a,b,*], Domenica Convertino [c], Neeraj Mishra [c,d], Camilla Coletti [c,d], Mauro Iodice [b], Franco Frasconi [e], Federico Pilo [e], Narcis Silviu Blaj [f], Daniele Paoloni [a,b], Ilaria Rago [g], Giovanni De Bellis [h,i], Gianluca Cavoto [g], Alessandro Ruocco [a,b]

[a] Dipartimento di Scienze, Università degli Studi di Roma Tre, Via della Vasca Navale 84, 00146 Rome, Italy
[b] INFN Sezione di Roma Tre, Via della Vasca Navale 84, 00146 Rome, Italy
[c] Center for Nanotechnology Innovation @NEST, Istituto Italiano di Tecnologia, Pisa, Italy
[d] Graphene Labs, Istituto italiano di tecnologia, Via Morego 30, I-16163 Genova, Italy
[e] INFN Sezione di Pisa, Edificio C, Largo B. Pontecorvo, 3 56127 Pisa, Italy
[f] Dipartimento di Matematica e Fisica, Università degli Studi di Roma Tre, Via della Vasca Navale 84, 00146 Rome, Italy
[g] Sapienza Università di Roma and INFN Sezione di Roma, Piazzale Aldo Moro 2, 00185 Rome, Italy
[h] Department of Astronautical, Electrical and Energy Engineering, Sapienza University of Rome, Via Eudossiana 18, 00184, Rome, Italy
[i] Research Center on Nanotechnology Applied to Engineering of Sapienza (CNIS), Sapienza University of Rome, Piazzale Aldo Moro 5, 00185, Rome, Italy

ARTICLE INFO

Keywords:
Graphene
Electron transmission
Plasmon
Electron energy loss spectroscopy
X-ray photoemission spectroscopy
Scanning electron microscopy

ABSTRACT

Here, we report on accurate transmission measurements of electrons below 1 keV through suspended monolayer graphene. Monolayer graphene was grown via chemical vapor deposition and transferred onto transmission electron microscopy (TEM) grids. A monochromatic electron gun has been employed to perform the measurements in the 30 – 900 eV range in ultra-high vacuum. The graphene transparency is obtained from the absolute measurement of the direct beam current and the transmitted one, by means of a Faraday cup. We observed a transmission going from ~20 to ~80% for monolayer graphene within the experimental electron energy range. The high quality and the grid coverage of the suspended graphene has been proved via micro-Raman, X-ray photoemission, electron energy loss spectroscopies and field-emission scanning electron microscopy. After a 550 °C in-vacuum annealing of the samples, the main contribution to the C 1s spectrum is due to the sp^2 component and the evidence of suspended monolayer graphene has been observed through the π-plasmon excitation.

1. Introduction

Graphene is a planar two-dimensional material made of sp^2 hybridized carbon atoms and arranged to form a honeycomb lattice. The properties of this material such as the mechanical strength, the thermal robustness and the electrical conductivity make it attractive in many different fields [1,2]. In particular, the transparency, and the attenuation length, of graphene and multilayer graphene for low-energy electrons (below 1 keV) is a topic of great interest in surface and nanostructure physics, as well as in high energy physics. The attenuation length [3] of slow electrons in solids involves several physical phenomena occurring at, or near, the surface. Several experimental techniques, such as photoemission, electron diffraction and scanning electron microscopy, are all influenced by electron-matter interaction. The so-called universal curve represents a historical attempt to summarize the electron interaction with all the materials [4]. Nevertheless, this curve does not work for all electron energies and material thicknesses. In fact, the band structure of a solid plays a major role in the propagation of electrons below 30 eV [5,6] and 2D materials require a different approach than bulk models [7]. Therefore, a deeper investigation of the electrons attenuation length for a few, or even a single, layers material is required. In this regard, graphene represents the typical case study.

The concept of graphene as a pressure-tight membrane transparent to electrons has also aroused the curiosity in the field of particle physics for the upgrade of existing detectors and the development of novel ones. The Micro Pattern Gaseous Detectors (MPGD), like GEM [8] or Micromegas [9], are employed in devices for the tracking of high energy ionizing particles or even for X-ray detection. The integration of suspended graphene over the holes of the Micromegas mesh (or over the holes of a GEM) presents several appealing aspects: transparency to electrons; removal of the ion back-flow; suitability for the use of different gases and/or different pressure conditions in

* Corresponding author at: Dipartimento di Scienze, Università degli Studi di Roma Tre, Via della Vasca Navale 84, 00146 Rome, Italy.
E-mail address: alice.apponi@uniroma3.it (A. Apponi).

https://doi.org/10.1016/j.carbon.2023.118502
Received 28 June 2023; Received in revised form 14 September 2023; Accepted 3 October 2023
Available online 6 October 2023

the amplification region [10,11]. Another promising application of graphene in neutrino physics is the support of atomic tritium and it is considered in the development of a novel telescope to measure the neutrino mass and eventually unveil the cosmological neutrino background (Ptolemy experiment [12–15]). The knowledge of the transmission through graphene of the tritium β-electrons, although at higher energy, is crucial for this experiment as well.

The graphene transparency to electrons in vacuum and in gas (and in presence of an high electric field) can of course be different and will need to be measured. However, the measurements in vacuum represent the reference for any further study. The measurements of the electron transmission in the energy range below 1 keV are not many, to the best of our knowledge. Geelen et al. [5] reported on measurements of the inelastic mean free path, *i.e.* the mean distance between two inelastic scattering events, in graphene for electrons up to 25 eV and Konvalina et al. [16] in the 200–800 eV range with steps of several tens of eV. The transmission through graphene has been also studied in low-energy electron microscopy and holography for the imaging of nanoscale objects. With triode setups Hassink and coworkers [17] provided a lower bound of 60% transparency almost constant in the 2–40 eV range and Li et al. [18] found a variation between 10% and 80% in the 300 eV–3 keV range. Mutus et al. [19] measured a 74% graphene transparency via point projection microscopy with 100 eV electrons. From the analysis of holographic images through mono- bi- and tri-layer graphene, Longchamp and coworkers [20] reported that graphene transmits 73% of 66 eV electrons. In the majority of the experiments, the graphene on grid is used as a gate (or anode) kept at potential in order to accelerate or focus the electrons. The graphene impermeability to atoms, other than the transparency to electrons, is a feature exploited by Kraus et al. [21] for ambient pressure photoelectron spectroscopy (APPES). They evaluated the electron transmission from the attenuation of photoemission signal from substrates half-covered with graphene, obtaining 34% for 138 eV electrons and 57% for 997 eV in the case of monolayer and 15% at 894 eV in the case of four-layer graphene. The measured energy range is extremely limited so far, thus the picture on the graphene transmission of low-energy electrons requires further studies to be exhaustive.

We present in this work accurate measurements of the electron transmission in the 30–900 eV range through monolayer graphene on a metallic TEM grid, in ultra-high vacuum (UHV). We carried out absolute measurements of the electron current, direct or transmitted. In our set-up both the grid with graphene and the exit electrode of the electron source are grounded, so that the electron flight is not affected by any electric field. Moreover, a thorough characterization of the graphene samples has been performed in order to check the quality and the grid coverage with both spectroscopic and microscopic techniques: micro-Raman, X-ray photoemission, electron energy loss spectroscopies and field-emission scanning electron microscopy.

2. Sample preparation and experimental methods

Polycrystalline monolayer graphene was synthesized at CNI@NEST laboratory in Pisa using a commercial cold-wall chemical vapor deposition (CVD) reactor (AIXTRON BM Pro) on electropolished copper foil (purity 99.99%, Alfa-Aesar) [22,23]. The optimization of this procedure, as thoroughly discussed in the Supplemental Material, guarantees the production of monolayer graphene above 90% with a small bilayer contribution. The graphene was then transferred on a TEM nickel grid (Ted Pella Inc. G2000HAN, 3-mm diameter, 2-μm thickness, nominal open area 41%, 6.5-μm nominal holes diameter, no lacey carbon) using the standard wet etching technique [22,24,25] (see Supplemental Material for more details on the sample preparation). Optical images acquired at different magnifications are shown in Fig. 1(a). The quality and integrity of the graphene membrane after the transfer on TEM grids were assessed by Raman spectroscopy [26,27]. A micro-Raman spectroscope (inVia Raman, Renishaw), equipped with a motorized sample stage, a 532 nm laser and a 50X long working distance objective, was used to map the entire grid with steps of 10 μm to check the characteristic graphene Raman peaks. The laser power was kept at 1 mW with an acquisition time of 1 s. The Raman maps confirmed the full coverage of graphene on the TEM grid and its high quality. In Fig. 1(b), the typical Raman spectrum for the monolayer graphene is shown. The spectrum is characterized by prominent G and 2D peaks and the negligible intensity of the D-peak confirmed the high crystal quality of the graphene [27].

The UHV chamber, hosted in the LASEC laboratory at Roma Tre University, is equipped with the apparatuses for electron transmission measurements, X-ray photoemission spectroscopy (XPS) and electron energy loss spectroscopy (EELS). The base pressure of the UHV chamber is $1 \cdot 10^{-9}$ mbar.

The source of electrons, for both the transmission and the EELS measurements, is a custom-made monochromatic electron gun with an energy resolution of 45 meV [28]. The electron energy can be tuned within the 30–900 eV range. The size of the beam is ~0.5 mm (full width at half maximum) within this energy range. Details about the method for the beam size evaluation can be found in [28,29]. Therefore, the graphene transparency is measured as an average on several TEM grid holes (6.5 μm nominal diameter). The beam current was about 200 pA for all the measurements reported in this work.

The absolute measurement of the current is performed by means of a Faraday cup and a B2987A Keysight picoammeter (0.1 fA resolution in the 200 pA range). The Faraday cup has a hole with a diameter of 3 mm, therefore the electron current is fully integrated. In order to measure the current transmitted through the graphene on the TEM grid, the latter is fitted on a drilled sample holder which can be mounted in front of the Faraday cup. In Fig. 2, a schematic layout for these measurements is shown on the left while the layout for XPS and EELS is depicted on the right. Details on the spectroscopic apparatuses are reported in Supplemental Material.

Field emission scanning electron microscopy (FE-SEM) has been carried out at CNIS (Research Center on Nanotechnology Applied to Engineering of Sapienza University) by collecting secondary electrons through a Zeiss Auriga SEM (Oberkochen, Germany) operated at an accelerating voltage of 2 keV, a working distance of 5.5 mm and using a 30 μm aperture. Micrographs were acquired at 500x and 5000x magnifications.

A 550 °C in-vacuum annealing has been performed in order to clean the sample from PMMA residues due to the graphene transfer on the TEM grid (see Supplemental Material for the evaluation of the residual thickness). This high-temperature in-vacuum annealing procedure is known to be effective for graphene surface cleaning [30,31].

All the measurements have been performed for two monolayer graphene samples (sample A and B) belonging to the same CVD growth and transferred onto commercial TEM grids of the same type. For the sample B we herein report only the results of the FE-SEM and transmission measurements.

3. Results and discussion

3.1. Electron spectroscopies

The C 1s core-level has been measured with XPS for the monolayer graphene before and after the in-vacuum annealing. The measured spectra are reported in Fig. 3, along with the fitting curves. In order to take into account the experimental resolution and the intrinsic line width, we employed Doniach-Sunjic profiles to fit the data.

In the as-prepared sample spectrum (Fig. 3(a)), the presence of several contributions other than the sp^2 component indicates graphene contamination due to PMMA residues ($C_5O_2H_8$), as deduced from measurements of a PMMA thin film [32]. After the 550 °C in-vacuum annealing, the main contribution to the C 1s spectrum (Fig. 3(b)) comes from the sp^2 component at 284.5 eV of binding energy with 0.1

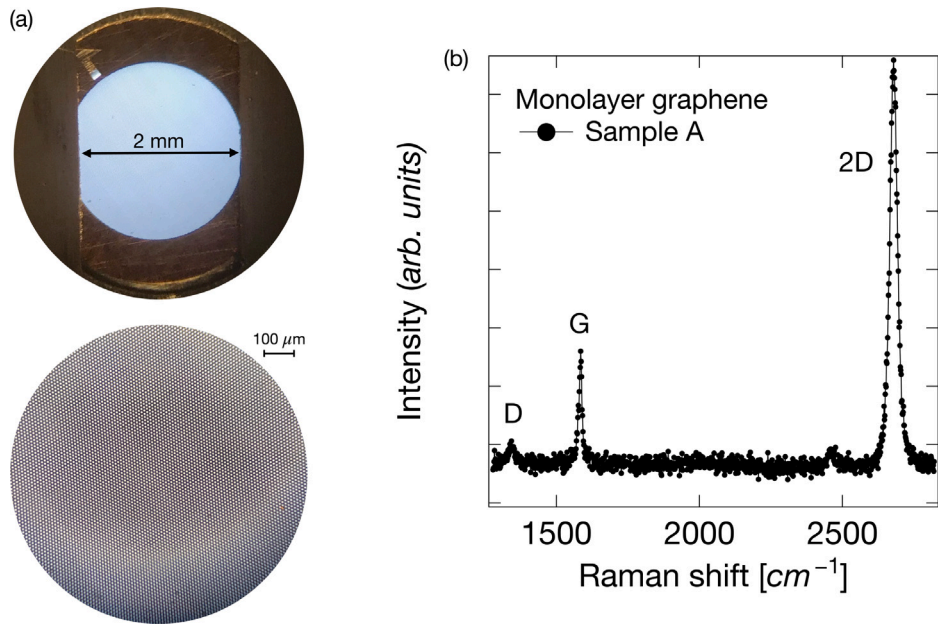

Fig. 1. (a) Optical images of the graphene on TEM grid sample as mounted on the carrier. The bottom image is acquired with higher magnification, as indicated by the scale bar. (b) Characteristic Raman spectrum of monolayer graphene transferred on TEM grid.

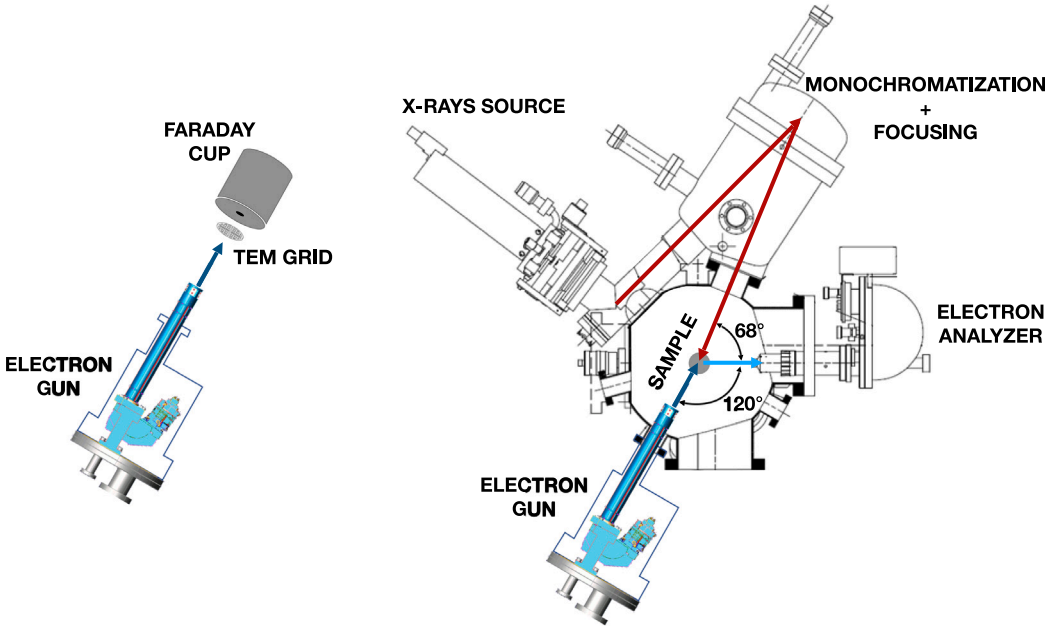

Fig. 2. On the left, a schematic layout for the measurements of the current emitted by the electron gun and transmitted through the graphene on TEM grid sample mounted in front of the Faraday cup (not to scale). On the right, a sketch of the experimental layout for XPS and EELS is reported. The X-ray beam monochromatized and focused on the sample is shown in red, the electron beam emitted by the gun toward the sample is depicted in dark blue and the photoelectrons entering the electron analyser are shown in light blue. (For interpretation of the references to colour in this figure legend, the reader is referred to the web version of this article.)

Doniach-Sunjic asymmetry. The Lorentzian width of this component resulted to be larger for the monolayer (0.6 eV) than for the typical value of graphite (0.2 eV). The larger width can be explained with the presence of two unresolved components shifted in binding energy by ~240 meV and due to monolayer graphene suspended or in interaction with the substrate [33]. Although this result reveals a purely planar sp^2 monolayer graphene, the high-temperature annealing breaks a large part of the graphene suspended on the grid holes, as assessed by the FE-SEM characterization on the annealed sample and further discussed. When reinserted in the experimental vacuum chamber after the FE-SEM measurements, a lower temperature annealing (400 °C) has been performed in order to clean the sample from adventitious contaminants due to the air exposure and preserve it from further breaks. The C 1s spectrum after the 400 °C annealing (Fig. 3(c)) is still dominated by the sp^2 component with a small amount (~3%) of CO contamination. The results of the fit analysis for monolayer graphene sample after 550 °C and 400 °C annealing are summarized in Table 1.

The EELS spectra have been measured with a primary electron energy of 91 eV. The measurement was focused on the π-plasmon collective excitation, which is supposed to be found at different energy losses if the graphene is suspended or in coordination with the substrate or with other graphene layers [34–36]. In Fig. 4(a) the measured energy loss spectra for the as-prepared and the 550 °C annealed monolayer graphene sample are shown. Before the in-vacuum annealing of the

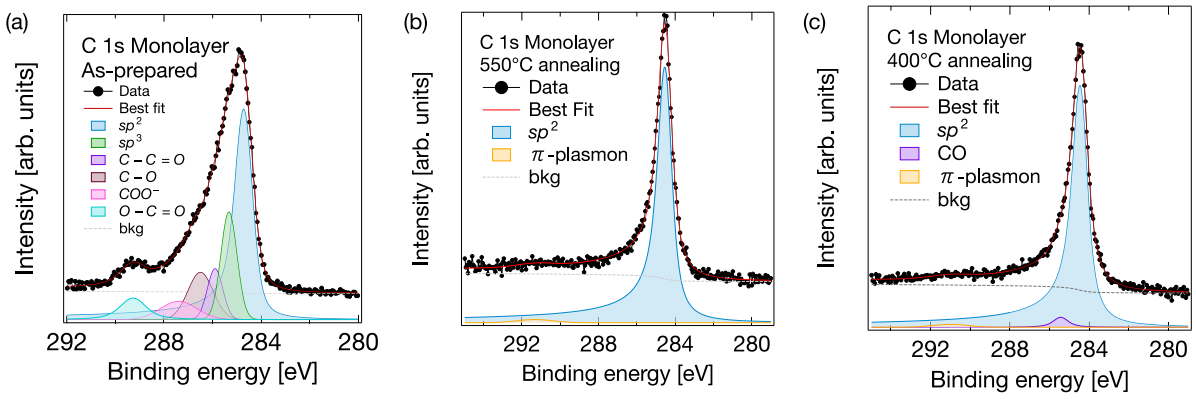

Fig. 3. XPS spectra of the C 1s core-level for monolayer graphene (a) as-prepared, (b) 550 °C annealed and (c) 400 °C annealed after air exposure. The black dots represent the experimental data, the red solid line is the sum of the fitting curves, the grey dashed line is the background and the Doniach-Sunjic profiles follow the colours reported in the legends. (For interpretation of the references to colour in this figure legend, the reader is referred to the web version of this article.)

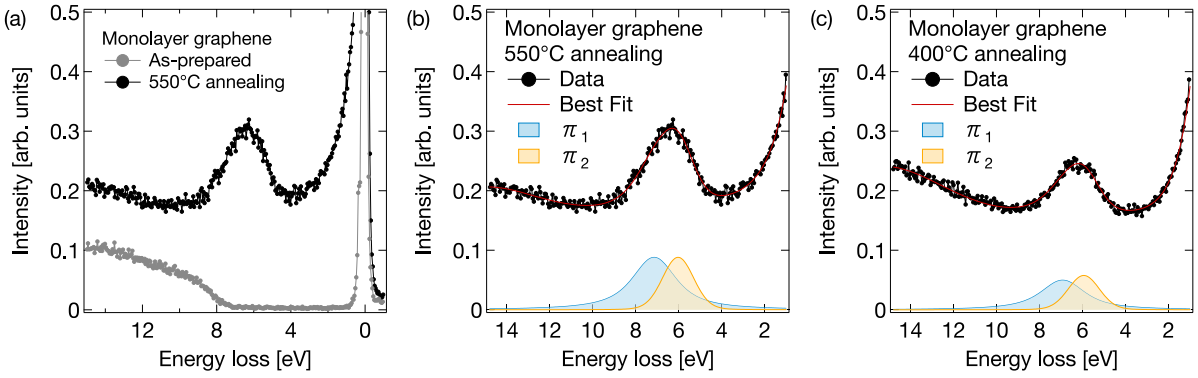

Fig. 4. (a) EELS spectra for the as-prepared (grey) and 550 °C annealed (black) monolayer graphene. The incident current for the two spectra is the same as well as the scale factor of the *y*-axis. Spectra around the π-plasmon excitation for the 550 °C (b) and 400 °C (c) annealed monolayer graphene sample, along with the fitting curves. In (b) and (c) the black dots represent the experimental data, the red solid line is the sum of the fitting curves, the π_1- and π_2- plasmon components are shown in blue and yellow respectively. (For interpretation of the references to colour in this figure legend, the reader is referred to the web version of this article.)

Table 1
Results of the fit analysis on the C 1s core-level measured for monolayer graphene sample after 550 °C and 400 °C annealing. Component name, binding energy, peak area, Gaussian width (GW), Lorentzian width (LW) and peak asymmetry are listed.

550 °C annealed monolayer graphene					
Component	Binding energy [eV]	Area	GW [eV]	LW [eV]	Asymmetry
sp^2	284.50	2.24	0.45	0.58	0.1
π-plasmon	290.90	0.04	2.2	0	0
400 °C annealed monolayer graphene					
Component	Binding energy [eV]	Area	GW [eV]	LW [eV]	Asymmetry
sp^2	284.42	2.98	0.45	0.63	0.1
CO	285.55	0.10	0.50	0.63	0
π-plasmon	291.00	0.05	2.10	0	0

Table 2
The results of the fit analysis on the EELS spectra for 550 °C and 400 °C annealed monolayer graphene samples are listed. Component name, energy loss, peak area, Gaussian width (GW) and Lorentzian width (LW) are listed.

550 °C annealed monolayer graphene				
Component	Energy loss [eV]	Area	GW [eV]	LW [eV]
π_1-plasmon	7.1	0.28	0.98	2.05
π_2-plasmon	6.0	0.17	1.62	0.17
400 °C annealed monolayer graphene				
Component	Energy loss [eV]	Area	GW [eV]	LW [eV]
π_1-plasmon	6.9	0.16	0.98	2.04
π_2-plasmon	5.9	0.11	1.62	0.17

monolayer sample the π-plasmon excitation (~6.5 eV) is completely quenched and the sample presents an insulator-like behaviour due to the PMMA residues and air contaminants. Once the sample is cleaned with the annealing, the appearance of the π-plasmon collective excitation is the evidence of long-range ordered sp^2 coordination of carbon atoms [37]. The spectra for the 550 °C and 400 °C annealed monolayer graphene sample along with the fitting curves are shown in Fig. 4(b) and (c) respectively. The results of the fit analysis are summarized in Table 2.

For both the 550 °C and 400 °C annealed monolayer graphene spectra, we found two contributions separated by ~1 eV each other. The presence of these two components can be explained by the fact that part of the monolayer graphene is coordinated with the nickel of the TEM grid, while the rest is suspended on the grid holes. On this basis, the π_1-plasmon excitation at higher energy loss is due to graphene in coordination with nickel and the π_2-plasmon, at energy loss 5.9 eV, to the suspended component. Considering that we perform EELS in the specular reflection condition, the inelastic scattering accompanied by an elastic event is the most probable process [38,39]. In this kinematic conditions, the momentum transferred is $|\mathbf{q}| \approx 0.2$ Å^{-1}. Given the measured π_2-plasmon energy loss and the momentum transferred, the result is highly consistent with what reported in [34].

3.2. Electron microscopy

The FE-SEM characterization, carried out on the monolayer graphene sample after the 550 °C annealing, revealed the breaking of

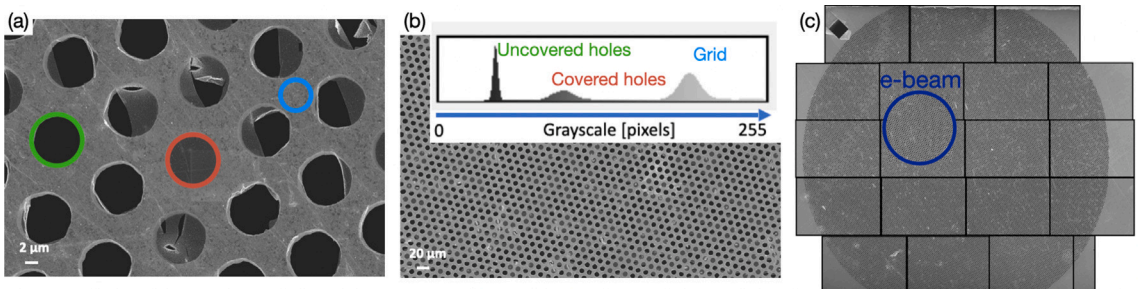

Fig. 5. (a) FE-SEM image of the 550 °C annealed graphene on TEM grid at 5 kX magnification. (b) One of the FE-SEM images of the sample map at 500 X magnification with an example of the greyscale histogram (right top). The colours of the circles in (a) match the tags of the peaks of the histogram in (b) and show examples of uncovered holes regions (green), regions of suspended graphene covering the holes (red) and grid regions (light blue). (c) Complete map of the sample at 500 X magnification and the electron beam spot, drawn to scale in blue, with the images stitched together. (For interpretation of the references to colour in this figure legend, the reader is referred to the web version of this article.)

a large part of the graphene suspended on the grid holes, as can be seen in Fig. 5(a). Before the high-temperature treatment the membrane integrity and the full graphene coverage on the grid were assessed by the micro-Raman mapping procedure, as already discussed. Therefore the fractures, running mainly along the single-crystal domain edges, can be ascribed to the strain due to the thermal expansion. In light of this observation, the actual fraction of grid holes covered by graphene ("coverage") was evaluated, together with the grid geometrical transmission (*i.e.* holes area over the total area). To this aim, a complete map of the sample was needed. The sample was divided into a matrix of 19 acquired FE-SEM images at fixed operation conditions. The SEM images were analysed with ImageJ [40] on the basis of the grey level of the single pixel. A greyscale histogram of the pixels is built and it presents three separated peaks. Each peak can be associated to the specific features of the original image, as shown in Fig. 5(a) and (b): the colours of the circles in (a) match the tags of the peaks of the histogram in (b). The uncovered holes regions (green) are associated to the darkest grey narrow peak, regions of suspended graphene covering the holes (red) are linked to the lighter grey peak and grid regions (light blue) are related to the lightest grey peak. The area of the covered holes, uncovered holes and grid regions can be directly obtained from the corresponding peak area on the histogram. Then the graphene coverage and geometrical transmission are evaluated. Being the analysis carried out on the basis of the pixels grey level, the contribution to the area of the suspended graphene (*i.e.* covered holes) comes from both full and partially covered holes. Because of the contrast changes often present on the edges of the broken suspended graphene, the graphene coverage has been evaluated by subtracting the area of the uncovered regions to the total holes area. Indeed, the darkest peak associated to the uncovered regions is narrow and well defined.

The geometrical transmission and the graphene coverage are crucial quantities for the measurement of the electron transmission through graphene, as well as the fine control of the beam hitting position. Being the diameter of the electron beam ~0.5 mm (FWHM) greater than a single SEM image, some of them were stitched into one. The analysis was carried out on the circular region where the electron beam hits the grid. Fig. 5(c) shows the complete map of the sample and the electron beam spot (to scale) where the images are stitched together. We found a geometrical transmission of (37 ± 1)% and a coverage of (38 ± 1)% for sample A. For sample B the geometrical transmission resulted to be (44 ± 1)% and the coverage (42 ± 1)%. The discrepancy with respect to the nominal geometrical transmission (41%) can be ascribed to the difference in the measured holes diameter.

3.3. Transmission measurements

The transmission of electrons through the graphene on TEM grid was determined by measuring the electron current as a function of the kinetic energy from 30 to 900 eV (we call this procedure *energy scan*). The Faraday cup (FC) is placed in the line of sight of the electron gun and a first energy scan is performed, without the sample, in order to measure the direct beam current. The energy scan is repeated with the sample mounted in front of the FC, thus measuring the transmitted current through the grid holes with or without the graphene. This measurement is performed by choosing the beam position at each energy step in order to match the region in which the coverage is evaluated (similar positioning procedure can be found in [28,29]). Finally another scan on the FC is performed, where the direct beam current is measured again. Both the terminal electrode of the gun and the FC are grounded, so that the electrons flight is not affected by any electric field. The two direct current measurements, before and after the one with the TEM grid, are crucial to determine the current stability during this three steps method. We define the current instability as the modulus of the difference between the two direct current measurements over their average. The current instability is at most 1.1% within the experimental energy range. Since the accuracy of the picoammeter is 0.5%, the total uncertainty on the current measurements is essentially 1.2%.

We define the *measured* transmission of electrons through the sample as $T_{meas} = I_{sample}/I_0$, where I_{sample} is the beam current measured with the sample in front of the FC and I_0 is the average of the two direct current measurements. The first measured sample was an empty TEM grid (same type used for the monolayer graphene transfer). This corresponds to a measurement of the geometrical transmission of the grid. For this sample, we found T_{meas} ~39% constant within the 30–900 eV range. This result guarantees the absence of spurious instrumental effects introduced in the transmission measurement as an average on several grid holes. Then, we measured T_{meas} for monolayer graphene on TEM grid. It is important to underline here that this does not correspond to the measurement of the graphene transparency, since both the geometrical transmission and coverage have not been taken into account yet. In Fig. 6(a), the T_{meas} for the as-prepared, 550 °C annealed and 400 °C annealed sample A is shown together with T_{meas} for the empty TEM grid. The uncertainty, computed from the direct and transmitted current measurements, is 2.4%. As expected, the transmission measured for sample A lies always below the 37% geometrical transmission of the grid (dashed line) evaluated through the SEM image analysis. A significant increase after contaminants removal and graphene fracture is observed, in particular at low kinetic energies. On the other hand, the curve remains essentially unaltered between the two annealing treatments, showing that no further ruptures were created with the second annealing at lower temperature.

In order to obtain the *net* transmission through monolayer graphene (T_G), the T_{meas} was corrected by taking into account the coverage and the geometrical transmission of the grid, both evaluated with the analysis of the SEM images. Because of the graphene fractures, the measured current is $I_{meas} = a[I_0 T_{grid} T_G] + b[I_0 T_{grid}]$, where a is the fraction of grid holes covered by graphene, T_{grid} is the grid geometrical

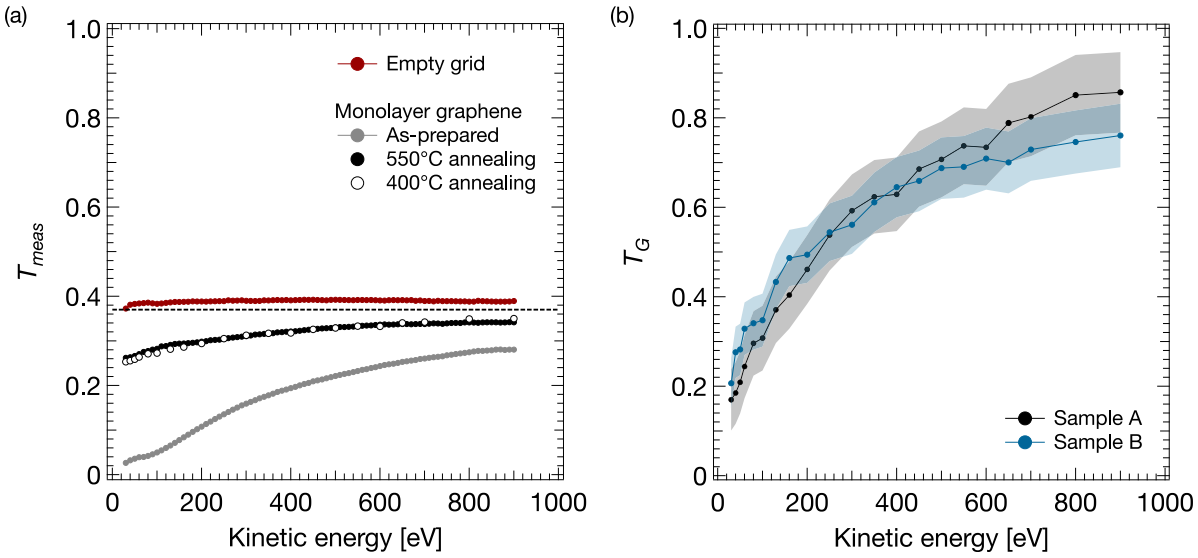

Fig. 6. (a) Measured transmission of electrons through an empty TEM grid (red) and through as-prepared (grey), 550 °C annealed (black markers) and 400 °C annealed (open markers) monolayer graphene on TEM grid. The dashed line is the 37% geometrical transmission of the TEM grid supporting the graphene, evaluated with SEM images analysis. (b) Corrected graphene transmission through the 400 °C annealed monolayer graphene (black) and a second annealed monolayer graphene (blue). The shaded areas represent the uncertainty associated with the respective T_G measurements. (For interpretation of the references to colour in this figure legend, the reader is referred to the web version of this article.)

transmission and b is the fraction of uncovered holes ($a + b = 1$). The first contribution represents the current passing through the suspended graphene, while the second is associated with the current passing through the uncovered regions of the grid holes. Thus, the corrected transmission through monolayer graphene is

$$T_G = \frac{\frac{I_{meas}}{I_0 T_{grid}} - b}{a}. \quad (1)$$

In Fig. 6(b), T_G for the 400 °C annealed samples A and B are shown in black and blue, respectively. The uncertainty on these measurements (shaded areas) was obtained by propagating the uncertainties on the current measurement and on the parameters evaluated with the SEM image analysis and these last are the dominating ones. Although the coverage and geometrical transmission are different for the two samples, within this uncertainty the two measurements resulted compatible. We found a monolayer graphene transmission of ~20% for 30 eV electrons growing up to ~80% for 900 eV electrons, within the experimental acceptance angle.

As discussed in Section 2 the monolayer graphene samples can present a bilayer contribution up to 10% which does not significantly affect the transmission measurements. Indeed, the uncertainty due to the evaluation of coverage and geometrical transmission is one order of magnitude greater than the variation associated to a 10% bilayer correction.

3.4. Comments on the transmission measurement

A few considerations on the nature of the measured transmitted electrons through the graphene on grid should be done at this point. In fact, the measured current may be due to both scattered (elastically and inelastically) and non scattered electrons. The FC is a device made of two concentric cups electrically decoupled. The external cup is in electric contact with the sample, has a semi-aperture of 21.5° and is always grounded, while the internal cup is responsible for the current measurement, has a semi-aperture of 12.4° and can be polarized. The measurements reported so far were performed with the FC totally connected to ground. In order to infer the amount of measured electrons scattered by graphene, we measured the transmitted current with 0 and 30 V of internal cup polarization, at fixed kinetic energy of 30 eV. The polarization of the internal cup has the effect of carrying in all the electrons scattered by the graphene within the 21.5° semi-aperture of the external cup. The difference of the current measured at 30 V and 0 V polarization is due only to scattered electrons within the solid angle between 12.4° and 21.5°. All the non scattered electrons travel straight toward the internal cup and are not affected by the polarization. Under the hypothesis of a uniform distribution of the scattered electrons within the solid angle between 0 and 21.5°, we can infer that the contribution of scattered electrons to the transmitted current is 11% at 0 V polarization (see Supplemental Material for a more detailed description). If a forward-peaked distribution is taken into account, the estimated contribution should be seen as an upper limit instead [41,42].

In order to evaluate the total scattering cross section for electrons interacting with graphene, one should measure all and only the non scattered electrons passing through graphene. Even though the contribution due to scattered electrons in our measurement is low, at least at low energy as emerged from the previous considerations, it is still not possible to derive the total scattering cross section. A deeper experimental investigation is required, and foreseen, in order to study the contribution and angular distribution of both elastically and inelastically scattered electrons. On the other hand, the evaluation of the effective attenuation length (Λ_{EAL}) is not possible by measuring only the transmitted current. By considering the Beer–Lambert law, the ratio d/Λ_{EAL} can be derived with d equal to the material thickness. However the thickness of a 2D material is an ill-defined quantity. Both graphite interlayer spacing (~3.35 Å) and twice the radius of the carbon sp^2 covalent bound (~2 × 1.46 Å) are commonly used as equivalent thicknesses for graphene [19,43]. The Λ_{EAL} extracted in this way is consequently affected by the arbitrariness of the choice (see Supplemental Material for the calculated values).

4. Conclusions

In this work, the transmission of electrons has been evaluated from the ratio of the current transmitted through graphene and the direct beam current, both measured with a Faraday cup. We observed that the

monolayer graphene transparency goes from ~20% for 30 eV electrons to ~80% for 900 eV electrons.

The accurate measurements reported herein fill the experimental gap in an extended energy region below 1 keV. We estimated that 89% of the transmitted current is due to non scattered electrons at 30 eV. In order to evaluate the total scattering cross section for the electron-graphene interaction, further investigations on the contribution of elastically and inelastically scattered electrons are required and foreseen.

The measured transparencies in this work represent a crucial first step in comprehending the potential uses of graphene layers in the upgrade of particle physics detectors. To assess the viability of graphene as a selective barrier in MPGD electrodes, additional measurements on the scattering components are necessary. These measurements should ideally be conducted under polarization with high electric fields, and finally moving from vacuum to gases. The extension of this technique of electron transmission measurement to even higher energy will pave the way to the use of graphene in targets for particle physics experiments.

CRediT authorship contribution statement

Alice Apponi: Methodology, Software, Formal analysis, Investigation, Data curation, Writing – original draft, Writing – review & editing , Visualization. **Domenica Convertino:** Investigation, Formal analysis, Writing – original draft, Writing – review & editing, Visualization. **Neeraj Mishra:** Investigation, Writing – review & editing. **Camilla Coletti:** Resources, Writing – review & editing, Supervision, Project administration, Funding acquisition. **Mauro Iodice:** Conceptualization, Validation, Resources, Writing – review & editing, Project administration, Funding acquisition, Supervision. **Franco Frasconi:** Writing – review & editing. **Federico Pilo:** Conceptualization, Writing – review & editing, Project administration. **Narcis Silviu Blaj:** Formal analysis, Software, Investigation. **Daniele Paoloni:** Formal analysis, Software, Writing – review & editing. **Ilaria Rago:** Investigation, Writing – review & editing. **Giovanni De Bellis:** Investigation, Writing – review & editing, Supervision. **Gianluca Cavoto:** Writing – review & editing, Funding acquisition, Resources, Validation. **Alessandro Ruocco:** Resources, Supervision, Project administration, Funding acquisition, Conceptualization, Methodology, Software, Validation, Writing – review & editing.

Declaration of competing interest

The authors declare that they have no known competing financial interests or personal relationships that could have appeared to influence the work reported in this paper.

Acknowledgements

We are grateful to Gianfranco Paruzza of the INFN Roma Tre Mechanical Workshop for his technical support. We gratefully acknowledge financial support from MUR, Italy PRIN 2020 project 2020Y2JMP5 ‘ANDROMeDa’. This project has received funding from the European Union’s Horizon 2020 research and innovation programme Graphene Flagship under grant agreement No. 881603. IR acknowledges the support of the Amaldi Research Center funded by the MIUR, Italy program ‘Dipartimento di Eccellenza’ (CUP: B81I18001170001).

Appendix A. Supplementary data

Supplementary material related to this article can be found online at https://doi.org/10.1016/j.carbon.2023.118502.

References

[1] D.G. Papageorgiou, I.A. Kinloch, R.J. Young, Prog. Mater. Sci. (ISSN: 0079-6425) 90 (2017) 75–127, URL https://www.sciencedirect.com/science/article/pii/S0079642517300968.

[2] K.S. Novoselov, A.K. Geim, S.V. Morozov, D. Jiang, M.I. Katsnelson, I.V. Grigorieva, S.V. Dubonos, A.A. Firsov, Nature (ISSN: 1476-4687) 438 (7065) (2005) 197–200.

[3] A. Jablonski, C.J. Powell, Surf. Sci. Rep. (ISSN: 0167-5729) 47 (2) (2002) 33–91.

[4] M.P. Seah, W.A. Dench, Surf. Interface Anal. 1 (1) (1979) 2–11, http://arxiv.org/abs/https://analyticalsciencejournals.onlinelibrary.wiley.com/doi/pdf/10.1002/sia.740010103. URL https://analyticalsciencejournals.onlinelibrary.wiley.com/doi/abs/10.1002/sia.740010103.

[5] D. Geelen, J. Jobst, E. Krasovskii, S. van der Molen, R. Tromp, Phys. Rev. Lett. 123 (8) (2019) 086802, (ISSN: 0031-9007, 1079-7114).

[6] A. Bellissimo, G.M. Pierantozzi, A. Ruocco, G. Stefani, O.Y. Ridzel, V. Astašauskas, W.S. Werner, M. Taborelli, J. Electron Spectrosc. Relat. Phenom. (ISSN: 03682048) 241 (2020) 146883.

[7] M. Xu, D. Fujita, J. Gao, N. Hanagata, ACS Nano 4 (5) (2010) 2937–2945, http://dx.doi.org/10.1021/nn100276w, PMID: 20373812.

[8] F. Sauli, Nucl. Instrum. Methods Phys. Res. A (ISSN: 0168-9002) 805 (2016) 2–24, Special Issue in memory of Glenn F. Knoll, URL https://www.sciencedirect.com/science/article/pii/S0168900215008980.

[9] Y. Giomataris, P. Rebourgeard, J. Robert, G. Charpak, Nucl. Instrum. Methods Phys. Res. A (ISSN: 0168-9002) 376 (1) (1996) 29–35, URL https://www.sciencedirect.com/science/article/pii/0168900296001751.

[10] P. Thuiner, R. Hall-Wilton, R.B. Jackman, H. Muller, T.T. Nguyen, E. Oliveri, D. Pfeiffer, F. Resnati, L. Ropelewski, J.A. Smith, M. van Stenis, R. Veenhof, 2014 IEEE Nuclear Science Symposium and Medical Imaging Conference (NSS/MIC), IEEE, Seattle, WA, ISBN: 978-1-4799-6097-2, 2014, pp. 1–4, URL http://ieeexplore.ieee.org/document/7431248/.

[11] S. Franchino, D. Gonzalez-Diaz, R. Hall-Wilton, R. Jackman, H. Muller, T. Nguyen, R. de Oliveira, E. Oliveri, D. Pfeiffer, F. Resnati, L. Ropelewski, J. Smith, M. van Stenis, C. Streli, P. Thuiner, R. Veenhof, Nucl. Instrum. Methods Phys. Res. A (ISSN: 01689002) 824 (2016) 571–574.

[12] A.G. Cocco, G. Mangano, M. Messina, J. Phys. Conf. Ser. (ISSN: 1742-6596) 110 (8) (2008) 082014, URL http://dx.doi.org/10.1088/1742-6596/110/8/082014.

[13] M.G. Betti, M. Biasotti, A. Boscá, F. Calle, N. Canci, G. Cavoto, C. Chang, A. Cocco, A. Colijn, J. Conrad, N.D. Ambrosio, N.D. Groot, P. de Salas, M. Faverzani, A. Ferella, E. Ferri, P. Garcia-Abia, I. García-Cortés, G.G. Gomez-Tejedor, S. Gariazzo, F. Gatti, C. Gentile, A. Giachero, J. Gudmundsson, Y. Hochberg, Y. Kahn, A. Kievsky, M. Lisanti, C. Mancini-Terracciano, G. Mangano, L. Marcucci, C. Mariani, J. Martínez, M. Messina, A. Molinero-Vela, E. Monticone, A. Moroño, A. Nucciotti, F. Pandolfi, S. Parlati, S. Pastor, J. Pedrós, C.P. de los Heros, O. Pisanti, A. Polosa, A. Puiu, I. Rago, Y. Raitses, M. Rajteri, N. Rossi, I. Rucandio, R. Santorelli, K. Schaeffner, C. Tully, M. Viviani, F. Zhao, K. Zurek, J. Cosmol. Astropart. Phys. 2019 (07) (2019) 047, URL https://doi.org/10.1088/1475-7516/2019/07/047.

[14] M.G. Betti, M. Biasotti, A. Boscá, F. Calle, J. Carabe-Lopez, G. Cavoto, C. Chang, W. Chung, A. Cocco, A. Colijn, J. Conrad, N.D. Ambrosio, P. de Salas, M. Faverzani, A. Ferella, E. Ferri, P. Garcia-Abia, G.G. Gomez-Tejedor, S. Gariazzo, F. Gatti, C. Gentile, A. Giachero, J. Gudmundsson, Y. Hochberg, Y. Kahn, M. Lisanti, C. Mancini-Terracciano, G. Mangano, L. Marcucci, C. Mariani, J. Martínez, M. Messina, A. Molinero-Vela, E. Monticone, A. Nucciotti, F. Pandolfi, S. Pastor, J. Pedrós, C.P. de los Heros, O. Pisanti, A. Polosa, A. Puiu, Y. Raitses, M. Rajteri, N. Rossi, R. Santorelli, K. Schaeffner, C. Strid, C. Tully, F. Zhao, K. Zurek, Prog. Part. Nucl. Phys. (ISSN: 0146-6410) 106 (2019) 120–131, URL https://www.sciencedirect.com/science/article/pii/S0146641019300080.

[15] A. Apponi, M. Betti, M. Borghesi, N. Canci, G. Cavoto, C. Chang, W. Chung, A. Cocco, A. Colijn, N. DÁmbrosio, N. de Groot, M. Faverzani, A. Ferella, E. Ferri, L. Ficcadenti, S. Gariazzo, F. Gatti, C. Gentile, A. Giachero, Y. Hochberg, Y. Kahn, A. Kievsky, M. Lisanti, G. Mangano, L. Marcucci, C. Mariani, M. Messina, E. Monticone, A. Nucciotti, D. Orlandi, F. Pandolfi, S. Parlati, C.P. de los Heros, O. Pisanti, A. Polosa, A. Puiu, I. Rago, Y. Raitses, M. Rajteri, N. Rossi, K. Rozwadowska, A. Ruocco, C. Strid, A. Tan, C. Tully, M. Viviani, U. Zeitler, F. Zhao, J. Instrum. 17 (05) (2022) P05021, URL https://doi.org/10.1088/1748-0221/17/05/p05021.

[16] I. Konvalina, B. Daniel, M. Zouhar, A. Paták, I. Müllerová, L. Frank, J. Piňos, L. Průcha, T. Radlička, W.S.M. Werner, E.M. Mikmeková, Nanomaterials (ISSN: 2079-4991) 11 (9) (2021) 2435.

[17] G. Hassink, R. Wanke, I. Rastegar, W. Braun, C. Stephanos, P. Herlinger, J.H. Smet, J. Mannhart, APL Mater. (ISSN: 2166-532X) 3 (7) (2015) 076106.

[18] C. Li, M.T. Cole, W. Lei, K. Qu, K. Ying, Y. Zhang, A.R. Robertson, J.H. Warner, S. Ding, X. Zhang, B. Wang, W.I. Milne, Adv. Funct. Mater. (ISSN: 1616301X) 24 (9) (2014) 1218–1227.

[19] J.Y. Mutus, L. Livadaru, J.T. Robinson, R. Urban, M.H. Salomons, M. Cloutier, R.A. Wolkow, New J. Phys. (ISSN: 1367-2630) 13 (6) (2011) 063011.

[20] J.-N. Longchamp, T. Latychevskaia, C. Escher, H.-W. Fink, Appl. Phys. Lett. 101 (11) (2012) 113117, (ISSN: 0003-6951, 1077-3118).

[21] J. Kraus, R. Reichelt, S. Günther, L. Gregoratti, M. Amati, M. Kiskinova, A. Yulaev, I. Vlassiouk, A. Kolmakov, Nanoscale 6 (23) (2014) 14394–14403, (ISSN: 2040-3364, 2040-3372).
[22] V. Miseikis, D. Convertino, N. Mishra, M. Gemmi, T. Mashoff, S. Heun, N. Haghighian, F. Bisio, M. Canepa, V. Piazza, C. Coletti, 2D Mater. 2 (1) (2015) 014006, URL https://doi.org/10.1088/2053-1583/2/1/014006.
[23] D. Convertino, F. Fabbri, N. Mishra, M. Mainardi, V. Cappello, G. Testa, S. Capsoni, L. Albertazzi, S. Luin, L. Marchetti, C. Coletti, Nano Lett. 20 (5) (2020) 3633–3641, http://dx.doi.org/10.1021/acs.nanolett.0c00571, PMID: 32208704.
[24] X. Li, W. Cai, J. An, S. Kim, J. Nah, D. Yang, R. Piner, A. Velamakanni, I. Jung, E. Tutuc, S.K. Banerjee, L. Colombo, R.S. Ruoff, Science 324 (5932) (2009) 1312–1314, https://www.science.org/doi/pdf/10.1126/science.1171245. URL https://www.science.org/doi/abs/10.1126/science.1171245.
[25] A.J. Marsden, M. Skilbeck, M. Healey, H.R. Thomas, M. Walker, R.S. Edwards, N.A. Garcia, F. Vuković, H. Jabraoui, T.R. Walsh, J.P. Rourke, N.R. Wilson, Phys. Chem. Chem. Phys. 24 (2022) 2318–2331, URL http://dx.doi.org/10.1039/D1CP04316A.
[26] A.C. Ferrari, J.C. Meyer, V. Scardaci, C. Casiraghi, M. Lazzeri, F. Mauri, S. Piscanec, D. Jiang, K.S. Novoselov, S. Roth, A.K. Geim, Phys. Rev. Lett. 97 (2006) 187401, URL https://link.aps.org/doi/10.1103/PhysRevLett.97.187401.
[27] L.G. Cançado, A. Jorio, E.H.M. Ferreira, F. Stavale, C.A. Achete, R.B. Capaz, M.V.O. Moutinho, A. Lombardo, T.S. Kulmala, A.C. Ferrari, Nano Lett. 11 (8) (2011) 3190–3196, http://dx.doi.org/10.1021/nl201432g, PMID: 21696186.
[28] A. Apponi, F. Pandolfi, I. Rago, G. Cavoto, C. Mariani, A. Ruocco, Meas. Sci. Technol. 33 (2) (2021) 025102, URL https://doi.org/10.1088/1361-6501/ac3d07.
[29] A. Apponi, G. Cavoto, M. Iannone, C. Mariani, F. Pandolfi, D. Paoloni, I. Rago, A. Ruocco, J. Instrum. 15 (11) (2020) P11015, URL https://doi.org/10.1088/1748-0221/15/11/p11015.
[30] B. Zhuang, S. Li, S. Li, J. Yin, Carbon (ISSN: 0008-6223) 173 (2021) 609–636.
[31] W. Xie, L.-T. Weng, K.M. Ng, C.K. Chan, C.-M. Chan, Carbon (ISSN: 0008-6223) 94 (2015) 740–748.
[32] S. Pletincx, K. Marcoen, L. Trotochaud, L.-L. Fockaert, J.M.C. Mol, A.R. Head, O. Karslioğlu, H. Bluhm, H. Terryn, T. Hauffman, Sci. Rep. (ISSN: 2045-2322) 7 (1) (2017) 13341.
[33] T. Susi, M. Scardamaglia, K. Mustonen, M. Tripathi, A. Mittelberger, M. Al-Hada, M. Amati, H. Sezen, P. Zeller, A.H. Larsen, C. Mangler, J.C. Meyer, L. Gregoratti, C. Bittencourt, J. Kotakoski, Phys. Rev. Mater. (ISSN: 2475-9953) 2 (7) (2018) 074005.
[34] M.K. Kinyanjui, C. Kramberger, T. Pichler, J.C. Meyer, P. Wachsmuth, G. Benner, U. Kaiser, Europhys. Lett. 97 (5) (2012) 57005, (ISSN: 0295-5075, 1286-4854).
[35] A. Generalov, Y. Dedkov, Carbon (ISSN: 00086223) 50 (1) (2012) 183–191.
[36] T. Eberlein, U. Bangert, R.R. Nair, R. Jones, M. Gass, A.L. Bleloch, K.S. Novoselov, A. Geim, P.R. Briddon, Phys. Rev. B 77 (23) (2008) 233406, (ISSN: 1098-0121, 1550-235X).
[37] G. Di Filippo, A. Liscio, A. Ruocco, Appl. Surf. Sci. (ISSN: 0169-4332) 512 (2020) 145605, URL https://www.sciencedirect.com/science/article/pii/S0169433220303615.
[38] A. Ruocco, M. Milani, S. Nannarone, G. Stefani, Phys. Rev. B 59 (1999) 13359–13364, URL https://link.aps.org/doi/10.1103/PhysRevB.59.13359.
[39] D.K. Saldin, Phys. Rev. Lett. 60 (1988) 1197–1200, URL https://link.aps.org/doi/10.1103/PhysRevLett.60.1197.
[40] C.A. Schneider, W.S. Rasband, K.W. Eliceiri, Nature Methods 9 (7) (2012) 671–675, (ISSN: 1548-7091, 1548-7105).
[41] A. Jablonski, F. Salvat, C.J. Powell, A.Y. Lee, NIST Electron Elastic-Scattering Cross-Section Database Version 4.0, NIST Standard Reference Database Number 64, National Institute of Standards and Technology, Gaithersburg, MD, 20899, 2016, URL https://srdata.nist.gov/srd64/.
[42] T. Ester, J. Kessler, J. Phys. B: At. Mol. Opt. Phys. 27 (18) (1994) 4295–4308, (ISSN: 0953-4075, 1361-6455).
[43] R.S. Weatherup, Top. Catalysis (ISSN: 1572-9028) 61 (20) (2018) 2085–2102.